Eur. Phys. J. D (2018) 72: 82
https://doi.org/10.1140/epjd/e2017-80413-2

THE EUROPEAN PHYSICAL JOURNAL D

Regular Article

Non-Maxwellian and magnetic field effects in complex plasma wakes*

Patrick Ludwig[1,a], Hendrik Jung[2], Hanno Kählert[1], Jan-Philip Joost[1], Franko Greiner[2], Zhandos Moldabekov[1], Jan Carstensen[3], Sita Sundar[1], Michael Bonitz[1], and Alexander Piel[2]

[1] Institut für Theoretische Physik und Astrophysik, Christian-Albrechts-Universität zu Kiel, Kiel, Germany
[2] Institut für Experimentelle und Angewandte Physik, Christian-Albrechts-Universität zu Kiel, Kiel, Germany
[3] ABB Switzerland Ltd., Baden-Dättwil, Switzerland

Received 15 June 2017
Published online 10 May 2018 –

Abstract. In a streaming plasma, negatively charged dust particles create complex charge distributions on the downstream side of the particle, which are responsible for attractive forces between the like-charged particles. This wake phenomenon is studied by means of refined linear response theory and molecular dynamics simulations as well as in experiments. Particular attention is paid to non-Maxwellian velocity distributions that are found in the plasma sheath and to situations with strong magnetic fields, which are becoming increasingly important. Non-Maxwellian distributions and strong magnetic fields result in a substantial damping of the oscillatory wake potential. The interaction force in particle pairs is explored with the phase-resolved resonance method, which demonstrates the non-reciprocity of the interparticle forces in unmagnetized and magnetized systems.

1 Introduction

Attractive, non-reciprocal forces between negatively charged dust particles in a plasma sheath had been experimentally verified already 20 years ago and were attributed to the accumulation of positive space charge in the wake of the particle [1,2] that arises from the focusing of the directed flow of positive ions by the highly-charged negative dust particle. The achieved understanding of ion-wake phenomena that was reached five years ago was summarized in two reviews [3,4], which give a comprehensive list of previous work in this field. Major challenges for the study of wake phenomena have arisen from new experiments in magnetized dusty plasmas [5,6] and from the necessity to transfer the results gained for ion wakes in quasineutral plasmas to the plasma sheath, which involves dc electric fields and non-Maxwellian distribution functions [7].

In this contribution, we review the progress made in the theoretical understanding and diagnostics of streaming complex plasmas and ion wakes within the SFB-TR24 in recent years [8–24]. In Section 2, the theory of ion wakes is outlined with emphasis on the adaptation of linear-response theory to magnetized and non-Maxwellian situations. Particular attention is paid to subsonic flows, which become increasingly important for experiments with dust particles confined in the presheath or bulk plasma [3,25,26]. In Section 3, the wake-mediated forces in particle pairs are studied by means of molecular dynamics simulations and experimentally with resonance measurements.

2 Theory of ion wakes

The question of studying streaming dusty plasmas with attractive wakefields theoretically, requires to go beyond the one-component plasma model [27–29] and to include non-equilibrium effects, especially the ion flow, explicitly. An accurate theoretical description of a non-ideal, multi-component complex plasma in non-equilibrium with vastly different time scales of the different particle species raises, however, a big challenge [9], and it turned out that a number of early reports were erroneous, see references [11,30] for details.

To achieve an accurate theoretical understanding of the fundamental interactions leading to collective behavior in a streaming plasma, detailed knowledge of the plasma wakefield is required. Its topology in the vicinity of the charged dust grain can be obtained from linear response (LR) theory including the effect of a directed ion flow, finite temperature, collisional and Landau damping as well as the effect of external electric and magnetic fields. Despite its linear character, the LR results show good agreement with PIC simulations [4], which include the response to all orders.

Assuming that the ion kinetic energy exceeds the dust–ion interaction energy, and that the ion dynamics are only

* Contribution to the Topical Issue "Fundamentals of Complex Plasmas", edited by Jürgen Meichsner, Michael Bonitz, Holger Fehske, Alexander Piel.

[a] e-mail: ludwig@theo-physik.uni-kiel.de

weakly affected by the dust,[1] the ion dynamics can be treated on the mean field level and by neglecting nonlinear effects. Consequently, the electrostatic potential of a single point-like grain screened by ions streaming with velocity $\mathbf{v}_\mathrm{d}$ becomes

$$\Phi(\mathbf{r}) = \frac{1}{(2\pi)^3} \int d^3\mathbf{k}\, \frac{\phi_\mathrm{C}(k)}{\epsilon(\mathbf{k}, \mathbf{k}\cdot\mathbf{v}_\mathrm{d})} e^{i\mathbf{k}\cdot\mathbf{r}}, \tag{1}$$

with $\phi_\mathrm{C}(k) = q_\mathrm{d}/\epsilon_0 k^2$ being the Fourier transform of the bare Coulomb potential and $\epsilon(\mathbf{k}, \omega) = 1 + \chi_\mathrm{i} + \chi_\mathrm{e}$ being the dynamic dielectric function.

The idea to use this potential for the dynamics of dust grains in a complex plasma was first realized by Murillo and co-workers [31] and by Joyce and Lampe [32]. They demonstrated that, in fact, wake effects and net attractive dust interactions can be reproduced by this approximation. Despite the success of this model, comparisons with PIC simulations revealed substantial quantitative discrepancies [30]. Therefore, we have developed an independent, highly optimized LR code Kielstream that allows for a high-precision numerical computation of 3D plasma wakefields and the resulting electric fields, see [9,11] for implementation details. MD simulations based on these LR potentials allow for studying the real dust dynamics, fully taking into account all dust–dust Coulomb correlations [33].

We consider electrons that are statically screened, i.e., $\chi_\mathrm{e} = (k\lambda_\mathrm{De})^{-2}$. The plasma wake is created by the motion of the ions relative to the dust with velocity v_d and fully determined by the following set of parameters:

– Mach number $M = v_\mathrm{d}/c_\mathrm{s}$;
– electron-to-neutral temperature ratio $T_\mathrm{en} = T_\mathrm{e}/T_\mathrm{n}$;
– ion-neutral scattering frequency $\nu_i = \tilde{\nu}_i/\omega_\mathrm{pi}$;

with the ion plasma frequency $\omega_\mathrm{pi} = (n_\mathrm{i} q_\mathrm{i}^2/\varepsilon_0 m_\mathrm{i})^{1/2}$, the ion sound speed $c_\mathrm{s} = (k_\mathrm{B} T_\mathrm{e}/m_\mathrm{i})^{1/2}$ (Bohm speed), and the thermal speed of neutrals, $v_\mathrm{th,n} = (k_\mathrm{B} T_\mathrm{n}/m_\mathrm{n})^{1/2}$. The results presented in Section 2.2 are given for a representative grain charge $q_\mathrm{d} = -10\,000\,e$ and $\nu_\mathrm{i} = 0.1$ [4].

We note that, in the LR approach, there are no free "fitting" parameters, resulting in a very good predictive power that is comparable to that of PIC simulations (within the applicability limits of LR). At the same time, LR provides valuable reference data as it does not suffer the noise and convergence problems of PIC codes (even for insufficiently low grid-resolutions), which often assume unrealistically large grain charges and, therefore, may exaggerate the contribution of nonlinear effects.

2.1 Ion susceptibility

The ion density response function (susceptibility) for a collisional Maxwellian plasma in an external magnetic field can be found in textbooks [34]. Based on this result and equation (1), we have conducted a comprehensive analysis of the dust-wake potential as a function of the ion

[1] This is not necessarily the case for all ions, in particular not in the vicinity of dust grains, and for slow ions.

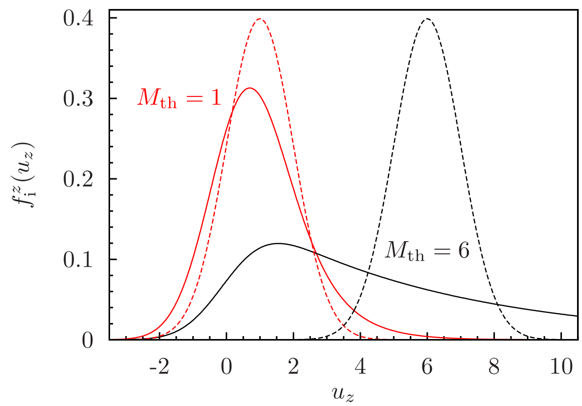

Fig. 1. Ion velocity distribution function in the streaming direction for two *thermal* Mach numbers $M_\mathrm{th} = M\sqrt{T_\mathrm{en}}$. The solid lines show the non-Maxwellian distribution [Eq. (2)] while the dashed lines are shifted Maxwellians.

magnetization [11], see Section 2.3. However, the ion distribution function in the sheath of discharges typically has a more complex shape. Ions are driven by the sheath electric field and undergo frequent collisions with the neutral gas, which often leads to strong deviations from a shifted Maxwellian [35]. In particular, using a reduced model, where the electric field is assumed to be constant, $\mathbf{E}_0 \equiv E_0\,\hat{\mathbf{e}}_z$, and only charge-exchange collisions are included, it could be shown that the velocity distribution along the streaming direction becomes much broader than a shifted Maxwellian [7]. This is illustrated in Figure 1, which shows a direct comparison between shifted Maxwellians and non-Maxwellian distributions that are obtained under the assumption that the ion-neutral collision frequency is constant (BGK model). The latter can be given in analytical form as [7]

$$f_\mathrm{i}^z(u_z) = \frac{1}{2M_\mathrm{th}} \exp\left(\frac{1 - 2\,M_\mathrm{th} u_z}{2\,M_\mathrm{th}^2}\right) \times \mathrm{erfc}\left(\frac{1 - M_\mathrm{th} u_z}{\sqrt{2}\,M_\mathrm{th}}\right), \tag{2}$$

where $u_z = v_z/v_\mathrm{th,n}$, and $M_\mathrm{th} = v_\mathrm{d}/v_\mathrm{th,n} = M/\sqrt{T_\mathrm{en}}$ is the *thermal* Mach number with the ion drift velocity $v_\mathrm{d} = q_\mathrm{i} E_0/(m_\mathrm{i}\tilde{\nu}_\mathrm{i})$.

The associated ion susceptibility, which includes the acceleration by the electric field and the nonequilibrium velocity distribution function, can be derived from kinetic theory [35,36]. We have recently extended these results to account for the effect of an additional external magnetic field $\mathbf{B}_0 || \mathbf{E}_0$ in order to investigate highly magnetized plasmas [10]. Two expressions for the susceptibility have been presented. The first includes a sum of Bessel functions and appropriately averaged plasma dispersion functions, while the second result can be expressed as the ratio of two integrals [10]

$$\chi_\mathrm{i}(\mathbf{k}, \omega) = \frac{1}{k^2 \lambda_\mathrm{i}^2} \frac{1 + A(\mathbf{k}, \omega)}{1 + B(\mathbf{k}, \omega)}, \tag{3}$$

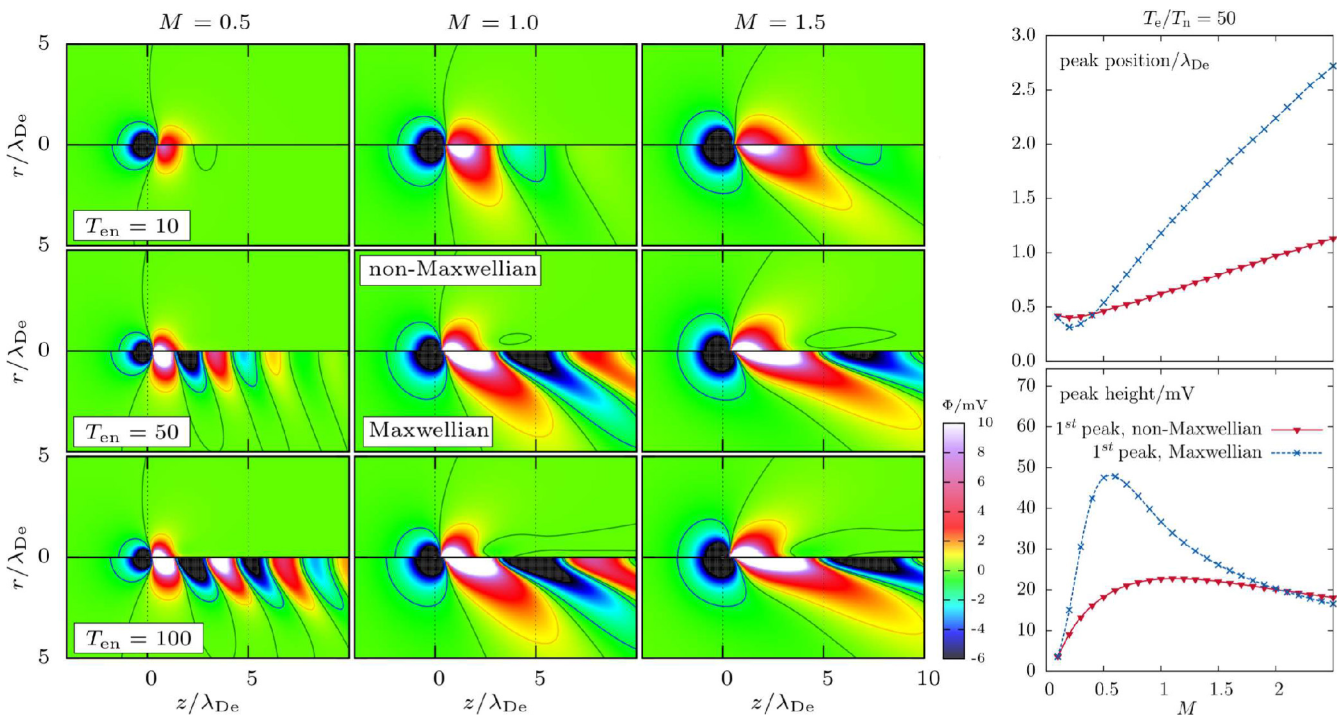

Fig. 2. Effect of temperature (*left panel*): contour plot of 3D dust potential $\Phi(r)$ for three different values of ion streaming velocity (from left to right: $M = 0.5, 1.0$ and $M = 1.5$) and three different temperature ratios $T_{\rm en}$ (increasing from top to bottom) at weak collisional damping $\nu_{\rm i} = 0.1$. The dust grain is located at the origin. Ions are streaming from left to right. Each graph is divided into an upper panel with non-Maxwellian ions and a lower panel with Maxwellian ions. Yellow/red to white (blue to black) colors correspond to positive (negative) potential values, respectively. *Right panel*: Position (top) and amplitude (bottom) of the trailing potential peak along flow direction as function of streaming velocity M for $T_{\rm en} = 50$. Red curves correspond to non-Maxwellian ions, blue curves to Maxwellian ions. The high amplitude of the trailing peak for subsonic streaming velocities in the Maxwellian case is strongly reduced for non-Maxwellian ions.

where $\lambda_{\rm i} = v_{\rm th,n}/\omega_{\rm pi}$. The functions A and B read

$$A(\mathbf{k},\omega) = \int_0^\infty \Lambda(\tau)\exp\left[\Psi(\tau)\right]\,d\tau,$$
$$B(\mathbf{k},\omega) = -\tilde{\nu}_{\rm i}\int_0^\infty \exp\left[\Psi(\tau)\right]\,d\tau. \tag{4}$$

The first integral involves

$$\Lambda(\tau) = \frac{i\left(\omega + i\tilde{\nu}_{\rm i} - k_z v_{\rm d}\tilde{\nu}_{\rm i}\tau\right)}{1 + ik_z v_{\rm d}\tau} - \frac{ik_z v_{\rm d}}{(1 + ik_z v_{\rm d}\tau)^2}, \tag{5}$$

and the exponential term is determined by

$$\Psi(\tau) = i(\omega + i\tilde{\nu}_{\rm i})\tau - k_z^2 v_{\rm th,n}^2 \frac{\tau^2}{2}\left(1 + \frac{i}{l_E k_z}\right) + \eta[\cos(\omega_{\rm ci}\tau) - 1]. \tag{6}$$

Here, $l_E = m_{\rm i} v_{\rm th,n}^2/(q_{\rm i}E_0)$ is a length scale associated with the electric field and $\omega_{\rm ci}$ the ion cyclotron frequency. For the Bessel form of the susceptibility, see reference [10].

In a different context, the influence of non-Maxwellian distributions on the ion-dust streaming instability was studied [12]. The largest deviations between the Maxwellian and the non-Maxwellian distribution were found at low to moderate ion-neutral damping. For streaming velocities below the ion sound speed, Maxwellian ions typically led to higher growth rates of the instability. However, the growth rates were found to decrease rapidly above $c_{\rm s}$ whereas they remained on a significant level in the non-Maxwellian case.

2.2 Non-Maxwellian effects in complex plasma wakes

A non-Maxwellian ion velocity distribution, obtained by taking the ion acceleration by an external electric field explicitly into account, leads to a completely different picture of the screened dust potential in a flowing plasma than a (shifted) Maxwellian ion distribution function, see Section 2.1. In comparison with previous results based on a shifted Maxwellian ion velocity distribution [4], we find that only one positive peak exists behind the dust grain, whereas the rest of the wake potential is largely suppressed.

In Figure 2, the screened grain potential is displayed for different values of the Mach number M (increasing from left to right) and temperature ratio $T_{\rm en}$ (increasing from top to bottom). The potential is highly anisotropic in streaming direction, but exhibits a cylindrical symmetry. Therefore, the upper half of each panel shows results for non-Maxwellian ions and the lower half for Maxwellian

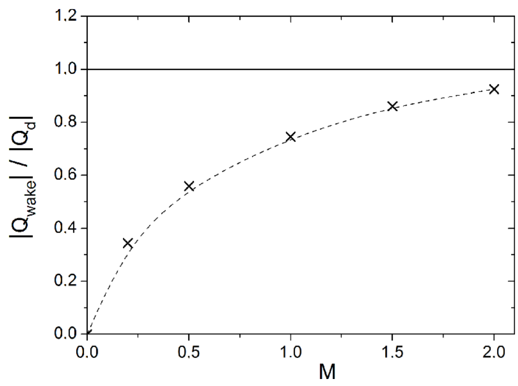

Fig. 3. Excess charge of the ion wake relative to the evoking charge of the dust grain for the collisionless case (non-Maxwellian ion distribution function, $T_{\rm en} = 100$) [24].

ions. For shifted Maxwellian ions, a strongly oscillating wakefield is found, even in the subsonic regime ($T_{\rm en} > 10$), which becomes more pronounced for a higher temperature ratio $T_{\rm en}$. The non-monotonic form of the potential gives rise to an effectively attractive interaction of two grains.

When the non-Maxwellian nature of ions is taken into account, oscillations are strongly suppressed: only a single positive (attractive) potential region develops in the wakefield of the dust grain, see also [37]. This finding is qualitatively similar to nonlinear PIC results: only the first minimum remains for non-Maxwellian ions, regardless of ion-neutral damping [23,38]. In general, the amplitude of the trailing peak is reduced and its position is located closer to the grain as compared to the Maxwellian case, as shown in the right panel of Figure 2 for $T_{\rm en} = 50$. Best agreement between both ion velocity distributions is found in the case of small values of M and $T_{\rm en}$.

Interestingly, our LR calculations show that wakefield effects become relevant even at relatively moderate ion flow velocities ($M \sim 0.3$). This behavior was also observed in experiments [26]. PIC simulations suggest, however, that wakefield effects disappear for $M \lesssim 0.3$ [25].

The characteristics of the induced ion density distribution around the grain charge will be discussed in an upcoming contribution [24]. As a preliminary result, we show the relation of the ion excess charge in the trailing wakefield compared to the charge of the evoking dust grain, for a non-Maxwellian ion distribution in the collisionless limit, see Figure 3. We find that with increasing M from 0.2 to 2, the wake charge increases monotonically from $0.34\, q_{\rm d}$ to $0.93\, q_{\rm d}$ and converges toward the dust particle charge which defines the upper bound. At sound speed, $M = 1$, the excess charge of the wake takes a value of 75% of the dust particle charge.

In Figure 4, the effect of collisional damping is explored (the temperature ratio is fixed at $T_{\rm en} = 100$). The middle row for $\nu_{\rm i} = 0.1$ corresponds to the lowest row in Figure 2. Reducing the damping frequency, i.e. $\nu_{\rm i} < 0.1$, has only a minor effect on the topology of the wakefield. The oscillation amplitude is slightly reduced, but the wavelength of the wakefield remains unchanged. When the damping frequency is increased, i.e. $\nu_{\rm i} > 0.1$, the long-ranging wakefield of the Maxwellian ions flattens out, and the wakefield's shapes of both distributions become similar, with a single pronounced trailing peak remaining.

What was first considered as numerical artifact [13], is the so-called *collision-induced wake amplification* [14,15], i.e., a growth of the wake amplitude with increase of the collision frequency $\nu_{\rm i}$, as seen in the right panel of Figure 4 in the range $\nu_{\rm i} < 0.1$ for non-Maxwellian ions. Subsequent studies reveal that this anomaly does appear in various classical and quantum systems as well as in ultrarelativistic plasmas [14,15]. The effect is also confirmed by independent PIC simulations, see [14,23] for details. We note that the non-Maxwellian model may become inapplicable at low ion-neutral damping and high streaming velocities due to an ion streaming instability [39].

2.3 Magnetic field effects in complex plasma wakes

Magnetized complex plasmas have been considered as the "next frontier for complex plasma research" [6]. Theoretically, the screened Coulomb potential in a flowing magnetized plasma has been studied in great detail for a shifted Maxwellian distribution of ions in reference [11]. However, as was shown before for the unmagnetized case, a non-Maxwellian ion distribution function leads to a considerably different wakefield compared to a shifted Maxwellian. Therefore, the density response function for streaming ions in parallel electric and magnetic fields was derived self-consistently, see Section 2.1. On that basis, LR calculations for magnetized complex plasmas have been carried out, where streaming ions interact with highly charged dust particles under the influence of a strong external magnetic field. The influence of the magnetic field is controlled by the dimensionless magnetization $\beta = \omega_{\rm ci}/\omega_{\rm pi}$.

An external magnetic field has a strong impact on the wakefield for $\beta > 0.5$, see Figure 5. As a general trend, for Maxwellian ions the amplitude and wavelength of the oscillating wakefield are reduced under the influence of a magnetic field [11], which is confirmed by experiments with strong magnetic fields [5]. The shape of the dynamically screened grain potential crucially depends on β and M: (i) for $M < 1$ the wake structure is bent in upstream direction forming half shells around the grain, which leads to strong potential oscillations lateral to the grain [see Fig. 6], (ii) for $M \geq 1$ the magnetic field suppresses the wake structure, which is compressed onto the flow axis. The potential lateral to the grain's position becomes monotonic.

For non-Maxwellian ions, distinct wakefield oscillations and off-axis extrema are largely suppressed. Only a single well-pronounced trailing potential maximum behind the dust grain is observed. At small M, the form of the positive potential peak (i.e., its equipotential lines) is bent upstream under the effect of the magnetic field, as observed for Maxwellian ions. At high Mach numbers and strong magnetization, screening becomes almost isotropic, as discussed in [11].

2.4 Wake effects in non-classical systems

The results obtained for non-ideal complex plasmas are of direct importance for other types of plasmas, e.g.,

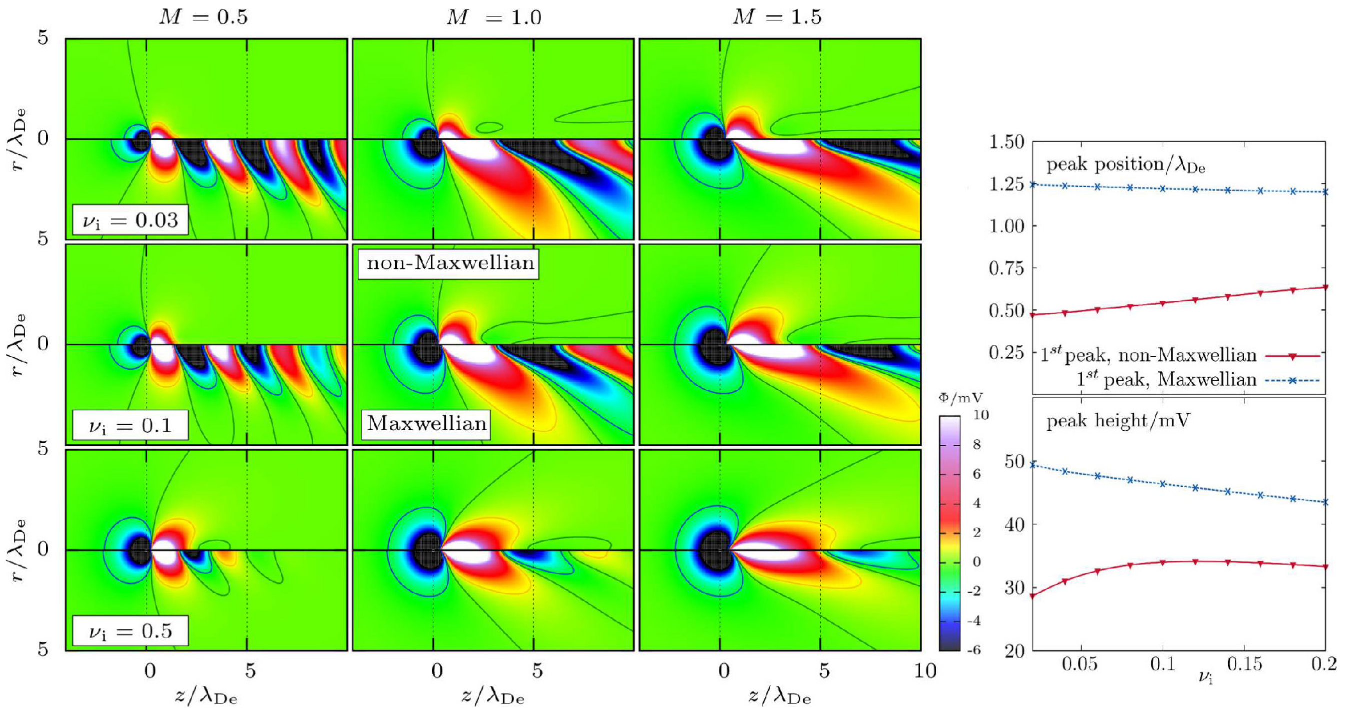

Fig. 4. Effect of collisional damping (*left panel*): dust potential $\Phi(r)$ with ions streaming from left to right as in Figure 2, but for three different collision frequencies $\nu_{\rm i}$ (increasing from top to bottom) and a fixed temperature ratio $T_{\rm en} = 100$. *Right panel*: Position (top) and amplitude (bottom) of the trailing potential peak along flow direction as function of collision frequency $\nu_{\rm i}$ ($M = 1$, $T_{\rm en} = 100$, cf. middle column in the left panel). Red curves correspond to non-Maxwellian ions, blue curves to Maxwellian ions. *Collision-induced wake amplification* is observed for $\nu_{\rm i} < 0.1$ for non-Maxwellian ions.

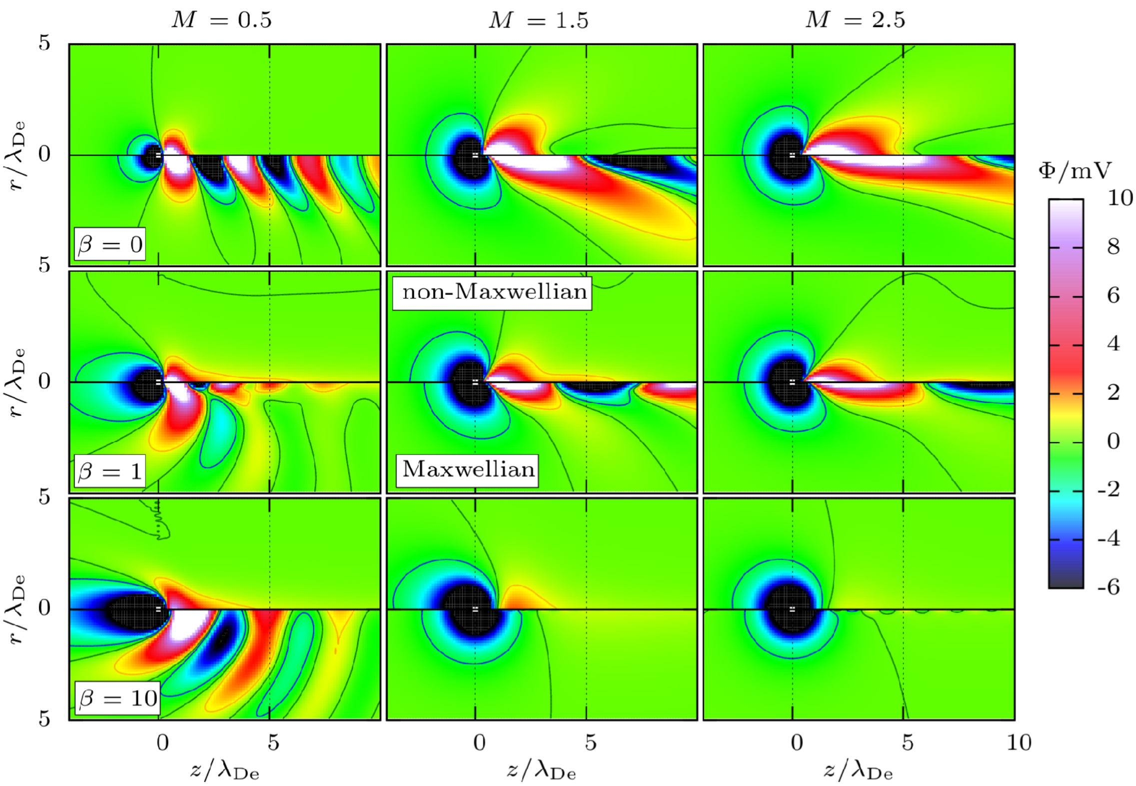

Fig. 5. Effect of an external magnetic field: dust potential $\Phi(r)$ with ions streaming from left to right as in Figure 2, but for different values of the Mach number M and a magnetic field applied along streaming direction (magnetization β is increasing from top to bottom). Temperature ratio $T_{\rm en} = 100$ and damping frequency $\nu = 0.1$ are fixed.

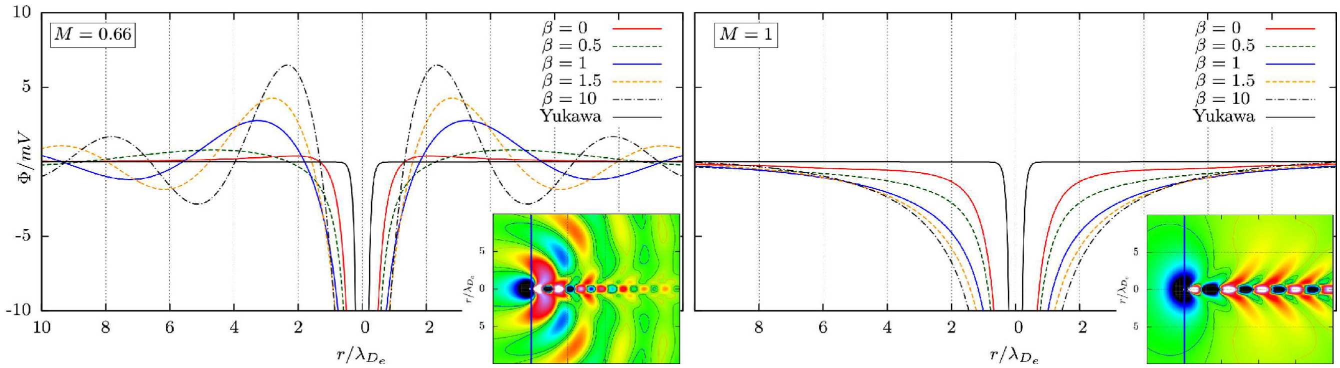

Fig. 6. Screened potential perpendicular to streaming direction at $z = 0$ (indicated by a blue line in the inset): in the subsonic regime at $M = 0.66$ (*left*) there are strong potential oscillations lateral to the grain that increase with β. At sound speed $M = 1$ (*right*) oscillations vanish and the potential is purely repulsive in lateral direction. Calculation for collisionless Maxwellian ions and $T_{\rm en} = 100$ (inset for $\beta = 1$). Adapted from [11].

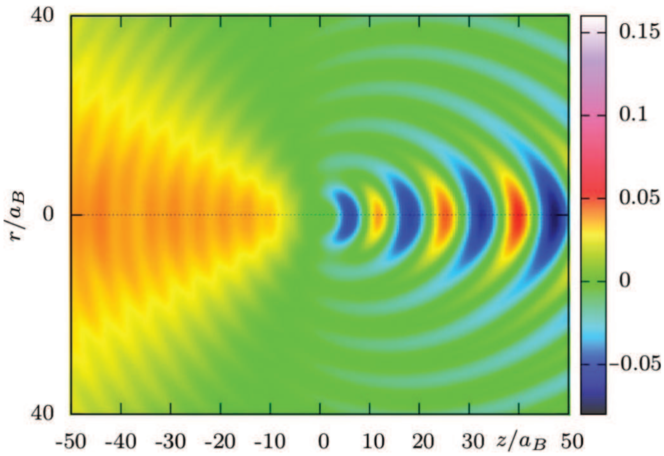

Fig. 7. Wake effect in an electron-ion quantum plasma: real space potential $|\mathbf{r}|^3\Phi(\mathbf{r})$ of a single ion moving (from right to left) in the presence of a degenerate electron plasma ($r_{\rm s} = 4.52$, $M = 0.5 v_{\rm F}$). From reference [13].

dense quantum plasmas (including so-called "warm dense matter") where streaming affects the mutual interplay of quantum degenerate electrons, classical ions and neutral atoms [40]. In this respect, the wake potential of a classical ion screened by *flowing quantum degenerate electrons* has been systematically investigated for values of the Brückner parameter in the range $0.1 \le r_{\rm s} \le 1$, where $r_{\rm s}$ is the ratio of the mean interparticle distance to the first Bohr radius, for a broad range of the plasma temperature and electron streaming velocity [13]. The resulting ion potential exhibits an oscillatory structure with attractive minima and, thus, strongly deviates from the static Yukawa potential of equilibrium plasmas, see Figure 7. The minimal electron streaming velocity for which attraction between ions occurs has been derived, which turns out to be less than the electron Fermi velocity $v_{\rm F}$. Our results allow for reliable predictions of the strength of wake effects in non-equilibrium quantum plasmas with fast streaming electrons showing that these effects are crucial for transport under warm-dense-matter conditions (i.e., at electron densities in the range of about $10^{24}\,{\rm cm}^{-3} \lesssim n \lesssim 10^{27}\,{\rm cm}^{-3}$ and temperatures $10^4\,{\rm K} \lesssim T \lesssim 10^6\,{\rm K}$ [13]), having strong impact for laser–matter interaction, electron-ion temperature equilibration, and stopping power. Particular attention also has been paid to anomalous quantum wake effects, that is, (i) the collision-induced wake amplification, and (ii) the non-monotonic temperature dependence of the wake amplitude [15]. For the sake of a broader picture, the appearance of plasma wake effects and their parametrical scaling has been evaluated and compared for classical, quantum, and ultrarelativistic plasmas [14].

2.5 Wake-mediated interparticle forces

Recently, a novel simulation method for the ion flow around dust particles with the "molecular asymmetric dynamics" (MAD) code was introduced [41]. There, the ion–ion interaction is described by a shielded potential while the highly charged dust is treated as an unshielded Coulomb potential. This approximation allows for a fast N-body calculation of all interparticle forces on the graphics processing unit. The MAD-code works best for large dust particles and is capable to study nonlinear wake effects. It has been critically compared with typical results from the SCEPTIC [42] and COPTIC [25] codes. Typical simulations use $N = 2^{16}$ superions in a spherical volume of $R = 3\lambda_{\rm De}$ radius.

A typical example for the wake-mediated interparticle forces in a pair of particles is shown in Figure 8. The ion flow is in $-z$ direction. The particle pair attains angular positions $\alpha = 0°–180°$ with the z direction at a fixed distance d. The particles have a radius $a = 25\,\mu$m and carry a fixed charge of $-169\,000$ elementary charges. The ions have a density $n_{\rm i} = 10^{14}\,{\rm m}^{-3}$ and a Mach number $M = 1$. The temperatures are $k_{\rm B}T_{\rm e} = 100\,k_{\rm B}T_{\rm i} = 2.5\,$eV.

The potential distribution in Figure 8a shows the formation of an overlapping wake pattern with a single positive hump on the downstream side. Right behind each of the two particles, distinctly separated maxima of the ion density are formed. The (dashed) density contours (1100, 1600, ..., 3100) $\lambda_{\rm De}^{-3}$ mark the enhanced ion density in the wake. The unperturbed ion density is $\approx 800\lambda_{\rm De}^{-3}$, typically.

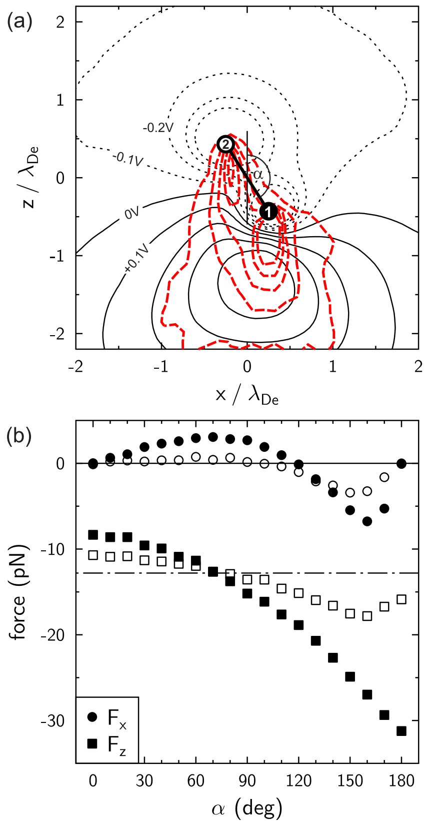

Fig. 8. MD-simulation of a particle pair at fixed distance d in an ion flow at $M = 1$ in $-z$ direction as a function of the orientation angle α with the z axis. (a) Potential contours (solid, dotted) and ion density contours (dashed) increasing $(1100, 1600, \ldots, 3100)\lambda_{\rm De}^{-3}$ at $d = \lambda_{\rm De}$, $\alpha = 150°$. (b) Force components for particle 1 as a function of orientation angle α. Full symbols: $d = \lambda_{\rm De}$, open symbols: $d = 2\lambda_{\rm De}$.

The force on particle 1 is shown in Figure 8b for $d = \lambda_{\rm De}$ (full symbols) and $d = 2\lambda_{\rm De}$ (open symbols). Since particle 1 is always to the right of particle 2, a positive horizontal force means repulsion, as found for $0° < \alpha < 120°$. A horizontal attractive force exists for $\alpha > 120°$. This happens, when particle 1 is close to the ion wake charge of particle 2, as shown in Figure 8a for $\alpha = 150°$. The same behavior is also found at the larger distance of $2\lambda_{\rm De}$.

The vertical force on particle 1 is always found negative. For comparison, the ion drag force on a single isolated particle under the same conditions, $F_{\rm id} = -12.8\,{\rm pN}$, is indicated by the dotted-dashed line. When particle 1 is atop of particle 2 ($\alpha = 0°$), the magnitude of the force is smaller than the reference value for the ion drag. This means that the net force from particle 2 and its wake pushes particle 1 upwards. This effect diminishes for increasing α. For $\alpha > 60°$, the force on particle 1 has a greater magnitude than the reference ion drag. This can be interpreted as an enhanced ion drag force from the combined focussing action of both particles. For the larger distance, the general trend is similar, except for $\alpha > 150°$, where the ion drag force of the isolated particle is approached.

Systematic studies of the forces for horizontal and vertical shifts in two-particle systems can be found in reference [41]. It was concluded that in a vertically aligned pair there is no net attractive force on the lower particle from the wake of the upper particle, because the lower particle experiences the repulsive Coulomb force from the upper particle and the difference of the attractive forces from ion accumulation above and below the lower particle. In summary, this example demonstrates the asymmetries and non-reciprocities of the wake-mediated forces in a two-particle system.

3 Wake diagnostics

The existence of a net attractive force between like-charged particles is remarkable and has two crucial consequences: (i) the dust system is non-Hamiltonian, (ii) the pair interaction is non-reciprocal: while the downstream particle is strongly affected by the dynamics of the upper grain, the upstream particle is only weakly affected by the lower one, see also [3,8] and references therein. Furthermore, a main effect of the wake formation is the enhanced ion flow on particles that are located in these wakes, which can lead to substantial changes of the particle charges [43].

3.1 Characterizing ion wake-induced particle properties by resonance measurements

Under experimental conditions, micrometer-sized dust particles can be confined in the lower plasma sheath of a capacitively coupled radio frequency (rf) discharge. There, the particles levitate due to the sheath electric field that compensates gravity. In addition to its inhomogeneous plasma environment, the sheath is determined by a field driven ion flow, which gives rise to the formation of ion wakes.

The simplest particle system for the investigation of wake effects is a vertically (parallel to the ion flow) aligned pair of particles. The phase-resolved resonance method (PRRM), which we had introduced in reference [44], is a well-proven high-precision technique to gain information on the charge-to-mass ratio and the size of single particles. Typical wake-induced characteristics of a particle pair, such as the asymmetric particle interaction and a reduced particle charge due to an enhanced ion flow to its surface, can be investigated. A detailed description of the method is given in reference [17]. The method relies on setting the dust particles into vertical oscillation by using external, periodical perturbations and analyzing their dynamical response. The external driver can be realized by either a modulated laser beam, a modulation of the self-bias, or a modulation of the rf power. In case of a vertically aligned pair of particles, the equations of motion are given by [43]:

$$\ddot{\xi}_{\rm u} + 2\gamma_{\rm u}\dot{\xi}_{\rm u} + \omega_{\rm u}^2\xi_{\rm u} + \frac{f_{\rm ud}}{m_{\rm u}}\left(\xi_{\rm u} - \xi_{\rm d}\right) = K_{\rm u}\exp(\mathrm{i}\omega t), \quad (7)$$

$$\ddot{\xi}_{\rm d} + 2\gamma_{\rm d}\dot{\xi}_{\rm d} + \omega_{\rm d}^2\xi_{\rm d} + \frac{f_{\rm du}}{m_{\rm d}}\left(\xi_{\rm d} - \xi_{\rm u}\right) = K_{\rm d}\exp(\mathrm{i}\omega t). \quad (8)$$

The index $j = \mathrm{u}, \mathrm{d}$ is used to identify the upstream and downstream particle, respectively. Resonance curves are obtained by measuring the excursion of the particles from their equilibrium positions ξ_j as a function of the driving frequency ω. This enables to determine the gas friction coefficient [45]

$$\gamma_j \propto \frac{1}{r_j \rho_j}, \tag{9}$$

which depends on the particle radius r_j and particle mass density ρ_j, as well as the charge-to-mass ratio of the particle that is given by the eigenfrequency ω_j of the harmonic confinement of the particles in the sheath:

$$\omega_j^2 \propto \frac{q_j}{m_j}. \tag{10}$$

Further, we obtain the stiffness parameter f_{jk}, which describes the strength of the particle interaction force that the particle k exerts on particle j.

An advantage of this method is that it allows to directly measure two typical wake-induced characteristics. Firstly, by comparing the eigenfrequency of the downstream particle, which is located in the wake of the upper one, with the eigenfrequency of an isolated single particle at the same position in the plasma sheath, the wake-induced charge reduction can be measured. It has been shown that the charge of a particle in the enhanced ion flow of the wake becomes significantly reduced by up to 20% [16,43]. Secondly, a comparison of the stiffness parameters in Figures 10 and 11 shows the wake-induced non-reciprocity of the particle interaction which is due to the natural asymmetry of the system of particles and their wake(s). The non-reciprocal interaction of a particle pair can attain values of $f_{\mathrm{du}} = (2\ldots 20)\, f_{\mathrm{ud}}$ [16,43].

3.2 Determining the spatial wake structure

The spatial wake structure of a dust grain in the flowing plasma environment of the plasma sheath has been studied experimentally [16]. A second lower particle has been continuously brought closer to the particle under investigation. The variable particle distance is realized by using a pair of particles with different masses and of different materials. Whereas the upper melamine formaldehyde (MF) particle is robust to plasma exposure and levitates at the same sheath position over a long time, the lower polymethyl methacrylate (PMMA) particle is strongly affected by plasma-inherent etching processes [16,46,47]. As shown in Figure 9, the continuous mass loss leads to a change of the charge-to-mass ratio and an increasing levitation height of the PMMA particle, resulting in a decreasing particle distance d.

Simultaneously performed resonance measurements do not only provide the time-resolved particle masses, which are determined from the measured gas friction coefficient γ_j [see Eq. (9)] [16,46], but also spatial information on the wake characteristics, namely the degree of asymmetry of the particle interaction forces and the charge reduction of the lower particle in the wake of the upper particle. In

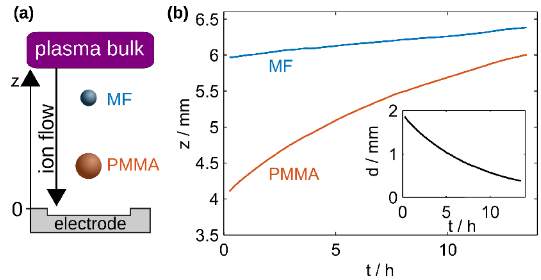

Fig. 9. (a) Sketch of the experimental situation: a MF particle and a larger PPMA particle are trapped in the lower plasma sheath. Due to its higher mass, the PMMA particle levitates below the MF grain. (b) Levitation height of both particles as a function of time. Mass losses of the PMMA particle lead to an increasing interparticle distance d. (Fig. (b) from Ref. [16].)

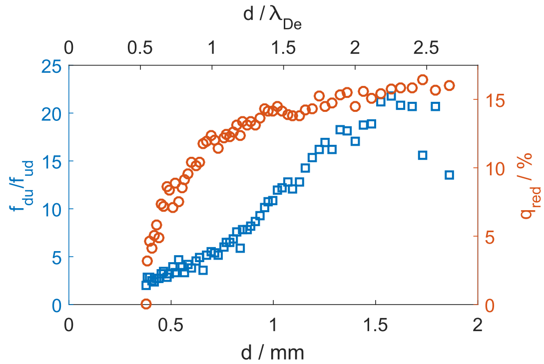

Fig. 10. Measured asymmetry of the particle interaction $f_{\mathrm{du}}/f_{\mathrm{ud}}$ (squares) and the degree of charge reduction of the lower particle q_{red} (circles) are shown as a function of the distance to the upper grain (at $d = 0$). Both quantities have a maximum in a distance of about $d \approx 1.5\,\mathrm{mm} \approx 2\lambda_{\mathrm{De}}$ and show no sign of a steep decrease at larger distances.

Figure 10, the results are shown as a function of the distance d to the upper grain. The closer the lower particle comes to the upper one, the more its charge approaches in the undisturbed case. Whereas its charge is reduced by up to 16% at larger distances; at small distances of $d \approx 0.5\,\mathrm{mm}$ it is almost unaffected. In addition, at small particle distances the degree of asymmetry of the particle interaction approaches symmetry, $f_{\mathrm{du}}/f_{\mathrm{ud}} = 1$. Large distances of more than 0.7 mm from the upper particle are characterized by a highly asymmetric particle interaction. This region with high charge reduction and strong asymmetric interaction can be directly related to the existence of the wake. Models use the electron Debye length λ_{De} of the bulk plasma and predict a maximum of the wake potential in a distance of 0.5–1.5 λ_{De} for $M \approx 1$ (see Sect. 2). The Debye length in the experimental situation is about $\lambda_{\mathrm{De}} \approx 0.7\,\mathrm{mm}$ [16], which means that the measured maximum of the wake characteristics are at a distance of about $2\,\lambda_{\mathrm{De}}$ (see Fig. 10). Nevertheless, the observed discrepancy – namely a more prolonged wake structure – can be attributed to the plasma environment in the sheath, which is not a homogeneous (quasineutral) flowing

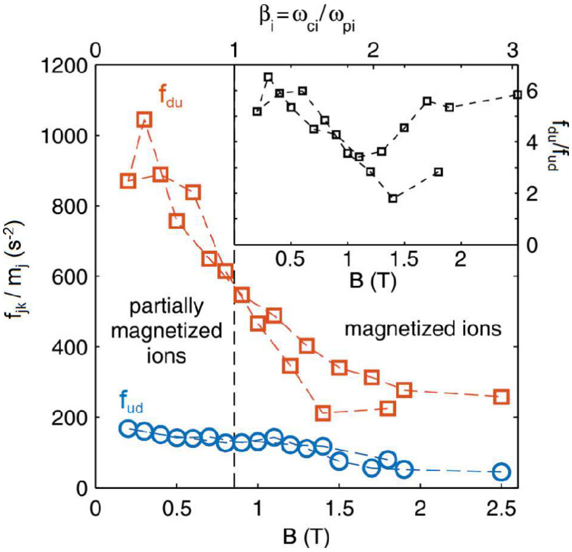

Fig. 11. Stiffness parameters f_{jka} of a vertically aligned pair of two almost same sized paricles as a function of the magnetic induction B. The magnetization of the streaming ions ($\beta_\mathrm{i} \geq 1$) leads to decreasing particle interaction forces. From reference [5].

plasma as it is the case in most models, but an inhomogeneous plasma with flowing ions, which are continuously accelerated by the sheath electric field. The experimental results are in very good accordance with theoretical predictions for wakes in the plasma sheath [48,49], which show a damping of the wake amplitude and a prolongation of the structure to one long extended wake maximum.

Another important result from the experiments is that for all situations where the particle is relatively close to the upper one ($d < 1\,\mathrm{mm}$),[2] the common notion [50] that the wake charge of the upper particle is located between the two grains does not hold for the situation of two particles in the plasma sheath. The majority of the wake charge is rather located underneath both particles, which is due to the fact, that the vertical particle positions are mainly given by the external confinement of the sheath, whereas the attractive forces of the wake play only a minor role [51].

3.3 Non-reciprocal particle interaction at strong magnetic fields

The influence of the plasma magnetization on the wake-induced particle interaction has been investigated by using a vertically aligned pair of almost same-sized MF particles [5]. A strong magnetic field with inductions of $B = (0.2 \ldots 2.5)\,\mathrm{T}$ is applied parallel to the ion flow.

Figure 11 shows the stiffness parameters of both parameters f_{jk} and their ratio which were measured with the PRRM at different magnetic inductions. The more the magnetic field is increased, the more the ions become magnetized ($\beta_\mathrm{i} > 1$). As shown, the magnetization of the ions at $\beta_\mathrm{i} \approx 1$ alters the longitudinal interparticle forces. This is in agreement with theoretical work which predicts a damping of the wake due to the plasma magnetization (see Sect. 2 and Ref. [52]).

Note that the trends of the parameters become very complex, if different levitation heights, different particle distances and/or varying particle masses are taken into account. In addition, the occurrence of plasma and particle instabilities are a major challenge for the investigation of dust at strong magnetic fields. These topics are part of current and prospective work.

[2] This is the case in all typical experiments, where two roughly same sized particles are used.

4 Conclusions

In this contribution, we have outlined recent progress and improvements for the dynamically screened Coulomb potential by taking into account effects of an external electric and/or magnetic field. Explicit consideration of the ion acceleration by an external electric field leads to a non-Maxwellian velocity distribution which gives rise to a completely different, strongly damped wakefield compared to the Maxwellian case. Solely the first trailing potential peak remains, which is located closer to the dust particle and has a lower amplitude. The effect of the collision-induced wake amplification has been identified, i.e., that a lower collision frequency can cause a stronger damped wake for non-Maxwellian ions.

Furthermore, we consider the situation where a magnetic field is aligned with the ion flow. In comparison with previous results based on a shifted Maxwellian ion velocity distribution [11], we find that only one positive potential peak behind the dust grain persists while the rest of the wake potential is largely suppressed.

Experimentally we have shown, how the structure of the wake behind a particle in the plasma sheath can be measured by using a second particle as a probe, which is continuously brought closer to the upper one. In the experiment, wake characteristics have been studied using the PRRM, which is based on evaluating the dynamical response of the particle system to small external perturbations. Wake characteristics as the non-reciprocal particle interaction and the charge reduction of a particle in the wake have been obtained as function of the particle distance by using particles of different materials. The experimental findings are consistent with the complex overlapping wake structures observed in MD-simulations (Fig. 8a and [41]). At strong magnetic fields parallel to the ion flow, the wake induced particle interaction is substantially damped.

This work is supported by the Deutsche Forschungsgemeinschaft via SFB-TR 24 (projects A2 and A9) and the German Academic Exchange Service (DAAD).

Author contribution statement

LR calculations were performed with Kielstream [9] by JPJ and ZhM, PIC-simulations with COPTIC [30] for comparisons by SS. Theoretical conception and analysis of simulations are in collaboration with PL, HK, and MB. The discussion of the ion susceptibility is contributed by

HK. MD-simulations are by AP. FG and AP conceived and evaluated the described experiments, which were prepared and performed by HJ and JC who also did the data analysis. The paper was written by PL, HJ, HK and AP. All authors contributed to the work and reviewed the final manuscript.

References

1. M. Nambu, S.V. Vladimirov, P.K. Shukla, Phys. Lett. A **203**, 40 (1995)
2. F. Melandsø, J. Goree, Phys. Rev. E **52**, 5312 (1995)
3. D. Block, J. Carstensen, P. Ludwig, W. Miloch, F. Greiner, A. Piel, M. Bonitz, A. Melzer, Contrib. Plasma Phys. **52**, 804 (2012)
4. P. Ludwig, W.J. Miloch, H. Kählert, M. Bonitz, New J. Phys. **14**, 053016 (2012)
5. J. Carstensen, F. Greiner, A. Piel, Phys. Rev. Lett. **109**, 135001 (2012)
6. E.J. Thomas, R.L. Merlino, M. Rosenberg, Plasma Phys. Control. Fusion **54**, 124034 (2012)
7. M. Lampe, T.B. Röcker, G. Joyce, S.K. Zhdanov, A.V. Ivlev, G.E. Morfill, Phys. Plasmas **19**, 113703 (2012)
8. A. Schella, A. Melzer, P. Ludwig, H. Thomsen, M. Bonitz, in *Complex plasmas: scientific challenges and technological opportunities*, edited by M. Bonitz, J. Lopez, K. Becker, H. Thomsen (Springer, New York, 2014), pp. 51–71
9. P. Ludwig, C. Arran, M. Bonitz, in *Complex plasmas: scientific challenges and technological opportunities*, edited by M. Bonitz, J. Lopez, K. Becker, H. Thomsen (Springer, New York, 2014), pp. 73–99
10. H. Kählert, J.P. Joost, P. Ludwig, M. Bonitz, Contrib. Plasma Phys. **56**, 204 (2016)
11. J.P. Joost, P. Ludwig, H. Kählert, C. Arran, M. Bonitz, Plasma Phys. Control. Fusion **57**, 025004 (2015)
12. H. Kählert, Phys. Plasmas **22**, 073703 (2015)
13. Z. Moldabekov, P. Ludwig, M. Bonitz, T. Ramazanov, Phys. Rev. E **91**, 023102 (2015)
14. Z.A. Moldabekov, P. Ludwig, J.P. Joost, M. Bonitz, T.S. Ramazanov, Contrib. Plasma Phys. **55**, 186 (2015)
15. Z.A. Moldabekov, P. Ludwig, M. Bonitz, T.S. Ramazanov, Contrib. Plasma Phys. **56**, 442 (2016)
16. H. Jung, F. Greiner, O.H. Asnaz, J. Carstensen, A. Piel, Phys. Plasmas **22**, 053702 (2015)
17. H. Jung, F. Greiner, O.H. Asnaz, J. Carstensen, A. Piel, J. Plasma Phys. **82**, 615820301 (2016)
18. A. Schella, M. Mulsow, A. Melzer, H. Kählert, D. Block, P. Ludwig, M. Bonitz, New J. Phys. **15**, 113021 (2013)
19. A. Melzer, A. Schella, M. Mulsow, Phys. Rev. E **89**, 013109 (2014)
20. A. Melzer, Phys. Rev. E **90**, 053103 (2014)
21. A. Schella, A. Melzer, C. July, C. Bechinger, Soft Matter **11**, 1197 (2015)
22. D. Block, W.J. Miloch, Plasma Phys. Control. Fusion **57**, 014019 (2015)
23. S. Sundar, H. Kählert, J.P. Joost, P. Ludwig, M. Bonitz, arXiv:1702.07152 (2017)
24. Z.A. Moldabekov, P. Ludwig, J.P. Joost, M. Bonitz, T.S. Ramazanov, arXiv:1709.09531 (2017)
25. I.H. Hutchinson, Phys. Rev. E **85**, 066409 (2012)
26. O. Arp, J. Goree, A. Piel, Phys. Rev. E **85**, 046409 (2012)
27. M. Bonitz, D. Block, O. Arp, V. Golubnychiy, H. Baumgartner, P. Ludwig, A. Piel, A. Filinov, Phys. Rev. Lett. **96**, 075001 (2006)
28. P. Ludwig, S. Kosse, M. Bonitz, Phys. Rev. E **71**, 046403 (2005)
29. M. Bonitz, C. Henning, D. Block, Rep. Prog. Phys. **73**, 066501 (2010)
30. I.H. Hutchinson, Phys. Plasmas **18**, 032111 (2011)
31. J.E. Hammerberg, D.S. Lemons, M.S. Murillo, D. Winske, IEEE Trans. Plasma Sci. **29**, 247 (2001)
32. G. Joyce, M. Lampe, G. Ganguli, IEEE Trans. Plasma Sci. **29**, 238 (2001)
33. P. Ludwig, H. Kählert, M. Bonitz, Plasma Phys. Control. Fusion **54**, 045011 (2012)
34. A.A. Rukhadze, A.F. Alexandrov, L.S. Bogdankevich, *Principles of plasma electrodynamics* (URSS, Moscow, 2013)
35. A.V. Ivlev, S.K. Zhdanov, S.A. Khrapak, G.E. Morfill, Phys. Rev. E **71**, 016405 (2005)
36. V. Schweigert, Plasma Phys. Rep. **27**, 997 (2001)
37. R. Kompaneets, G.E. Morfill, A.V. Ivlev, Phys. Rev. E **93**, 063201 (2016)
38. I.H. Hutchinson, C.B. Haakonsen, Phys. Plasmas **20**, 083701 (2013)
39. R. Kompaneets, A.V. Ivlev, S.V. Vladimirov, G.E. Morfill, Phys. Rev. E **85**, 026412 (2012)
40. P. Ludwig, M. Bonitz, H. Kählert, J.W. Dufty, J. Phys.: Conf. Ser. **220**, 012003 (2010)
41. A. Piel, Phys. Plasmas **24**, 033712 (2017)
42. I.H. Hutchinson, Plasma Phys. Control. Fusion **48**, 185 (2006)
43. J. Carstensen, F. Greiner, D. Block, J. Schablinski, W.J. Miloch, A. Piel, Phys. Plasmas **19**, 033702 (2012)
44. J. Carstensen, H. Jung, F. Greiner, A. Piel, Phys. Plasmas **18**, 033701 (2011)
45. P.S. Epstein, Phys. Rev. **23**, 710 (1924)
46. J. Carstensen, F. Haase, H. Jung, B. Tadsen, S. Groth, F. Greiner, A. Piel, IEEE Trans. Plasma Sci. **41**, 764 (2013)
47. O.H. Asnaz, H. Jung, F. Greiner, A. Piel, Phys. Plasmas **24**, 083701 (2017)
48. L.J. Hou, Y.N. Wang, Z.L. Mišković, Phys. Rev. E **68**, 016410 (2003)
49. R. Kompaneets, A.V. Ivlev, V. Nosenko, G.E. Morfill, Phys. Rev. E **89**, 043108 (2014)
50. A. Melzer, V.A. Schweigert, A. Piel, Phys. Rev. Lett. **83**, 3194 (1999)
51. V. Nosenko, A.V. Ivlev, R. Kompaneets, G. Morfill, Phys. Plasmas **21**, 113701 (2014)
52. M. Salimullah, M. Torney, P.K. Shukla, A.K. Banerjee, Phys. Scr. **67**, 534 (2003)